Contribution from the Department of Chemistry,
University of Houston—University Park, Houston, Texas 77004

Electrochemistry of Indium(III) Porphyrins in Pyridine and in Dichloromethane/Pyridine and Dichloromethane/*N*-Methylimidazole Mixtures

J.-L. Cornillon, J. E. Anderson, and K. M. Kadish*

Received December 20, 1985

The electrochemistry of indium porphyrins was studied in pyridine, dichloromethane/pyridine, and dichloromethane/*N*-methylimidazole mixtures. Complexes of (P)InX were investigated where P is the dianion of either octaethylporphyrin (OEP) or tetraphenylporphyrin (TPP) and X is an anionic ligand such as SO_3Ph^-, $SO_3CH_3^-$, Cl^-, or acetate (OAc^-). The neutral (P)InX complexes can form hexacoordinated species in the presence of the nitrogenous bases, and the reduction potentials and reduction mechanisms for these species are reported. The specific electrode reactions that occur depend upon the specific anion bound to In(III) as well as on the strength and concentration of the nitrogenous base in solution. The singly reduced metalloporphyrins are able to form either a mono(nitrogenous base) adduct with or without the loss of X^-, or, alternatively, a bis(nitrogenous base) adduct with the concomitant loss of X^-. The doubly reduced metalloporphyrins are invariably pentacoordinated in solution, and in the presence of nitrogenous bases, $[(P)In(L)]^{2-}$ is formed after the addition of two electrons. Equilibrium constants for ligand-addition and ligand-substitution reactions of the neutral and reduced indium porphyrins were studied as a function of potential sweep rate, temperature, and the concentrations of X^-, pyridine, or imidazole in solution. On the basis of these data an overall oxidation-reduction sequence is postulated for different types of experimental conditions.

Introduction

Ligand-binding reactions of metalloporphyrins have been extensively investigated over the last dozen years.[1,2] Four-, five-, or six-coordinate metalloporphyrin complexes may be present in solution, but the specific coordination geometry of the complex will depend upon the solvent system and the type and strength of the axial ligand, as well as the type of metal ion and its oxidation state. Transition-metal metalloporphyrins of oxidation states +3 and +2 almost invariably form six-coordinate complexes in the presence of imidazole or pyridine.[1,2] In contrast, only one imidazole or pyridine ligand is generally added to main-group metalloporphyrins with metals in the +2 oxidation state. A six-coordinate THF adduct of (TPP)Zn (where TPP = the dianion of tetraphenylporphyrin) has been structurally characterized,[3] but no additional six-coordinate Zn(II) porphyrins have ever been identified.[4-6] Likewise, (TPP)M complexes of Cd(II) and Hg(II) as well as those of Cu(II) form only monoadducts with nitrogeneous bases.[6-8]

Ligand-binding reactions of main-group metalloporphyrins in a +3 oxidation state have not been investigated in great detail except for the case of indium complexes.[10] The chemistry and reactivity of In(III) porphyrins are of recent interest.[11-16] Indium porphyrins of the type (P)InX[17-21] and (P)In(R)[16,22-24] have been well characterized, but until recently,[10] no monomeric six-coordinate indium(III) porphyrins had been spectrally observed. With weak-field ligands such as SO_3Ph^- or $SO_3CH_3^-$ facile dissociation of the anion may occur with the concomitant formation of a six-coordinate species.[10]

Six-coordinate species are also observed for the reactions of *N*-methylimidazole with acetate and chloro In(III) metalloporphyrins.[10] These ligand-addition reactions are given by eq 1-3

$$(P)InX + L \overset{K_1}{\rightleftharpoons} (P)InX(L) \quad (1)$$

$$(P)InX(L) + L \overset{K_2}{\rightleftharpoons} [PIn(L)_2]^+ + X^- \quad (2)$$

$$(P)InX + 2L \overset{\beta_2}{\rightleftharpoons} [(P)In(L)_2]^+ + X^- \quad (3)$$

where P is the dianion of tetraphenylporphyrin (TPP) or octaethylporphyrin (OEP), X is an anionic ligand such as SO_3Ph^-, $SO_3CH_3^-$, Cl^-, or acetate (OAc^-), and L is either *N*-MeIm or py.

The largest binding constants ($\beta_2 \geq 10^8$) are observed for the reaction of *N*-methylimidazole with In(III) complexes containing weakly bound anionic ligands such as SO_3Ph^- and $SO_3CH_3^-$. Pyridine binds more weakly to the In(III) center than *N*-MeIm, and only (P)InSO_3Ph and (P)InSO_3CH_3 give spectroscopic evidence for pyridine binding. For these complexes, β_2 for eq 3 is greater than or equal to 10^6.

In this paper, we report the detailed electron-transfer and ligand-exchange reactions of In(III) porphyrins that occur in neat pyridine or in CH_2Cl_2 containing pyridine or *N*-methylimidazole. Eight porphyrin complexes have been selected for investigation. These are (P)InSO_3CH_3, (P)InSO_3Ph, (P)InCl, and (P)InOAc. As will be shown, the electrochemical behavior of (P)InX in the presence of pyridine or *N*-MeIm is very different from the electrochemical behavior in CH_2Cl_2. The singly and doubly reduced porphyrins readily bind with pyridine or *N*-MeIm, and this leads to a significantly different mechanism from that observed for the reduction of (P)InX in noncomplexing media.[14]

The electrochemistry of each (P)InX complex was performed in a variety of conditions. Fast scan rates and low temperatures were utilized in order to determine the electron-transfer mecha-

(1) *The Porphyrins*; Dolphin, D., Ed.; Academic: New York, 1978.
(2) *Porphyrins and Metalloporphyrins*; Smith, K. M., Ed.; Elsevier: New York, 1975.
(3) Schauer, C. K.; Anderson, O. P.; Eaton, S. R.; Eaton, G. R. *Inorg. Chem.* **1985**, *24*, 4082.
(4) (a) Kirksey, C. H.; Hambright, P. *Inorg. Chem.* **1970**, *9*, 958. (b) Kirksey, C. H.; Hambright, P.; Storm, C. B. *Inorg. Chem.* **1969**, *8*, 2141.
(5) Nappa, M.; Valentine, J. S. *J. Am. Chem. Soc.* **1978**, *100*, 5075.
(6) Kadish, K. M.; Shiue, L. R. *Inorg. Chem.* **1982**, *21*, 3623.
(7) Miller, J. R.; Dorough, G. D. *J. Am. Chem. Soc.* **1952**, *74*, 3977.
(8) Leggett, D. J.; Kelly, S. L.; Shiue, L. R.; Wu, Y. T.; Chang, D.; Kadish, K. M. *Talanta* **1983**, *30*, 579.
(9) Kadish, K. M.; Shiue, L. R. *Inorg. Chem.* **1982**, *21*, 1112.
(10) Cornillon, J.-L.; Anderson, J. E.; Kadish, K. M. *Inorg. Chem.* **1986**, *25*, 991.
(11) Cocolios, P.; Moise, C.; Guilard, R. *J. Organomet. Chem.* **1982**, *228*, C43.
(12) Cocolios, P.; Chang, D.; Vittori, O.; Guilard, R.; Moise, C.; Kadish, K. M. *J. Am. Chem. Soc.* **1984**, *106*, 5724.
(13) Onaka, S.; Yamashita, M.; Tatematsu, Y.; Kato, Y.; Goto, M.; Ito, T. *Inorg. Chem.* **1985**, *24*, 1070.
(14) Kadish, K. M.; Cornillon, J.-L; Cocolios, P.; Tabard, A.; Guilard, R. *Inorg. Chem.* **1985**, *24*, 3645.
(15) Kadish, K. M.; Boisselier-Cocolios, B.; Cocolios, P.; Guilard, R. *Inorg. Chem.* **1985**, *24*, 2139.
(16) Cocolios, P.; Guilard, R.; Bayeul, D.; Lecomte, C. *Inorg. Chem.* **1985**, *24*, 2058.
(17) Buchler, J. W.; Eikelman, G.; Puppe, L.; Rohbock, K.; Schneehage, H. H.; Weck, D. *Justus Liebigs Ann. Chem.* **1971**, *745*, 135.
(18) Bhatti, M.; Bhatti, W.; Mast, E. *Inorg. Nucl. Chem. Lett.* **1972**, *8*, 133.
(19) Eaton, S. S.; Eaton, G. R. *J. Am. Chem. Soc.* **1975**, *97*, 3660.
(20) Guilard, R.; Cocolios, P.; Fournari, P.; Lecomte, C.; Protas, J. *J. Organomet. Chem.* **1979**, *168*, C49.
(21) Cocolios, P.; Fournari, P.; Guilard, R.; Lecomte, C.; Protas, J. Boubel, J. C. *J. Chem. Soc., Dalton Trans.* **1980**, 2081.
(22) Cocolios, P.; Guilard, R.; Fournari, P. *J. Organomet. Chem.* **1977**, *129*, C11.
(23) Cocolios, P.; Guilard, R.; Fournari, P. *J. Organomet. Chem.* **1979**, *179*, 311.
(24) Lecomte, C.; Protas, J.; Cocolios, P.; Guilard, R. *Acta Crystallogr., Sect. B: Struct. Crystallogr. Cryst. Chem.* **1980**, *B36*, 2769.

0020-1669/86/1325-2611$01.50/0

nisms and to evaluate the kinetic parameters associated with several rate-determining processes. In addition, the equilibrium constants of ligand-addition reactions to the singly reduced $[(P)InX]^-$ and the doubly reduced $[(P)InX]^{2-}$ complexes were determined. These reactions are given by eq 4–6, where $[(P)InX]^-$,

$$[(P)InX]^- + L \overset{K_1^-}{\rightleftharpoons} [(P)InX(L)]^- \quad (4)$$

$$[(P)InX(L)]^- + L \overset{K_2^-}{\rightleftharpoons} (P)In(L)_2 + X^- \quad (5)$$

$$[(P)InX]^{2-} + L \overset{K_1^{2-}}{\rightleftharpoons} [(P)In(L)]^- + X^- \quad (6)$$

$[(P)InX(L)]^-$, and $(P)In(L)_2$ represent In(III) complexes of the porphyrin π anion radical and $[(P)InX]^{2-}$ and $[(P)In(L)]^-$ represent In(III) complexes of the porphyrin dianion.

Experimental Section

Cyclic voltammetric measurements were obtained with the use of a conventional three-electrode system. The working electrode was platinum button (A = 0.8 mm^2). A commercial saturated calomel electrode typically was the reference electrode, but in some cases a silver wire was used as a pseudoreference electrode. The reference electrode, in either case, was separated from the bulk solution by a fritted-glass bridge. When a silver-wire pseudoreference electrode was used, the potentials were referenced to the Fc/Fc^+ couple. Either an EG&G Model 173 potentiostat, an EG&G Model 175 Universal Programmer, and a Houston Instruments Model 2000 X-Y recorder or a BAS 100 Electrochemical Analyzer was used for cyclic voltammetric experiments. Controlled-potential electrolysis was performed with an EG&G Model 173 potentiostat or a BAS 100. Both the reference electrode and the platinum-grid counter electrode were separated from the bulk solution by means of a fritted-glass bridge. Unless otherwise noted, 0.10 M supporting electrolyte was used for electrochemical experiments.

The electronic absorption spectra of the neutral complexes were monitored in order to ascertain when ligation occurred under given experimental conditions. UV–visible spectra were measured by using an IBM 9430 spectrophotometer with matched 1-cm quartz cells.

Chemicals. Tetrabutylammonium perchlorate ($(TBA)ClO_4$) was recrystallized twice from ethanol. Tetrabutylammonium chloride ((TBA)Cl) and tetrabutylammonium acetate ((TBA)OAc) were recrystallized from acetone/ethyl ether mixtures under an inert atmosphere. The three supporting electrolytes were dried under vacuum and stored under nitrogen. HPLC grade methylene chloride (CH_2Cl_2) and ACS grade pyridine (py) were distilled over CaH_2 prior to use. The pyridine distillation was carried out under an N_2 atmosphere. N-Methylimidazole (N-MeIm) was distilled under vacuum and stored under an argon atmosphere. Syntheses of the (P)InX complexes have been reported elsewhere.[10]

Methods. Formation constants were evaluated by using a combination of spectral and electrochemical methodologies. Stability constants for addition of pyridine or N-MeIm to the neutral (P)InX complexes were calculated by the Benesi–Hildebrand method[25] while stability constants for the singly and doubly reduced complexes were determined by using electrochemical methodologies. This latter method involves a monitoring of the shift in $E_{1/2}$ values as a function of ligand concentration and has been discussed in the literature.[26]

Results and Discussion

Electrochemistry of $(P)InSO_3R$, $(P)InSO_3R(N\text{-MeIm})$, and $[(P)In(N\text{-MeIm})_2]^+$ in CH_2Cl_2. N-Methylimidazole strongly binds to $(P)InSO_3Ph$, and $(P)InSO_3Ph(N\text{-MeIm})$ is formed in CH_2Cl containing 1 equiv of N-MeIm. This was demonstrated by ^1H NMR, electronic absorption spectroscopy, and by conductivity-monitored titrations of $(P)InSO_3Ph$ with N-MeIm.[10] The electrochemistry supports these interpretations and, in addition, gives information about the singly and doubly reduced complexes.

The reduction of $(TPP)InSO_3Ph$ in CH_2Cl_2 containing various N-MeIm concentrations is shown in Figure 1. In the absence of N-MeIm, $(TPP)InSO_3Ph$ undergoes two reversible one-electron reductions ($E_{1/2}$ = −1.07 and −1.47 V). These reductions are labeled processes I and II in Figure 1a. Similar potentials are observed for the reduction of other (TPP)InX complexes in the same solvent/supporting electrolyte system.[14] A summary of the electrochemical data of $(P)InSO_3R$ is presented in Table I. The addition of 0.8 equiv of N-MeIm (Figure 1b) leads to the appearance of two new reductions (peaks III and IV) while the addition of 1.0 equiv of N-MeIm (Figure 1c) results in an almost complete disappearance of original peaks I and II as $(P)InSO_3Ph(N\text{-MeIm})$ is formed. Finally, after the addition of 4 equiv of N-MeIm, only two reversible waves are present. Further additions of N-MeIm to these solutions does not lead to the appearance of new waves but rather to shifts in the half-wave potentials for peaks III and IV. (See Figure 1d for the shift observed after 85 equiv.) From the spectroscopic data,[10] the species in solution is $[(TPP)In(N\text{-MeIm})_2]^+$ at an N-MeIm to porphyrin ratio of more than 6:1. Thus, peak III, at larger concentrations of N-MeIm, is due to the reduction of $[(TPP)In(N\text{-MeIm})_2]^+$.

Analyses of the half-wave potentials for peaks III and IV were carried out as a function of the N-MeIm concentration and gave plots similar to those shown in Figure 2. In this figure, the shift of the half-wave potentials for peaks III and IV can be separated into two regions of ligand concentration. These are region A, which ranges from a log (N-MeIm) of −3.0 to −2.2 and region B, which ranges from a log (N-MeIm) of −2.20 to −0.20. In region A, $E_{1/2}$ for the first reduction (peak III) shifts by −66 mV with each tenfold increase in N-MeIm concentration, but the $E_{1/2}$ for the second reduction (peak IV) has only a slight dependence on the N-MeIm concentration. In region B, the first reduction (peak III) does not shift with an increase in the N-MeIm concentration

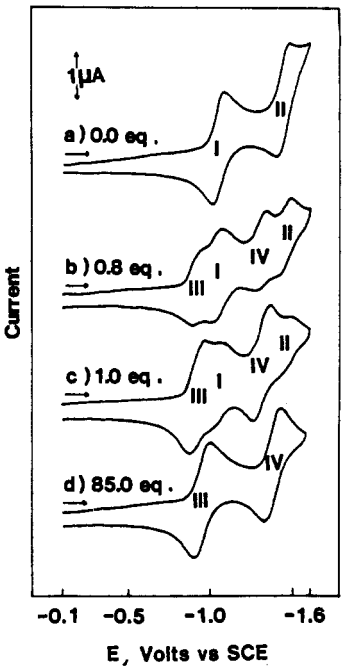

Figure 1. Cyclic voltammograms of 0.6×10^{-3} M $(TPP)InSO_3Ph$ in CH_2Cl_2, 0.1 M $(TBA)ClO_4$ containing the following equivalents of N-MeIm: (a) 0.0; (b) 0.8; (c) 1.0; (d) 85.0.

Table I. Half-Wave (V vs. SCE) for the First and Second Reductions of (P)InX in Various Solutions Containing 0.1 M $(TBA)ClO_4$[a]

initial porphyrin	CH_2Cl_2		CH_2Cl_2 + 1 M N-methylimidazole		pyridine	
$(TPP)InSO_3Ph$	−1.07	−1.47	−0.99	−1.44	−0.77	−1.30
$(TPP)InSO_3CH_3$	−1.07	−1.47	−0.99	−1.44	−0.77	−1.30
(TPP)InCl	−1.09	−1.48	−0.99	−1.45	[b]	−1.30
(TPP)InOAc	−1.12	−1.49	−1.00	−1.45	[b]	1.30
$(OEP)InSO_3Ph$	−1.30	−1.81[c]	−1.23		−1.04	−1.64
$(OEP)InSO_3CH_3$	−1.30	−1.82[c]	−1.23		−1.04	−1.64
(OEP)InCl	−1.29	−1.72	−1.23		[b]	−1.64
(OEP)InOAc	−1.32	−1.82[c]	−1.25		[b]	−1.64

[a] See text for reactions. [b] See text. [c] E_p at scan rate = 0.10 V/s.

(25) Benesi, H. A.; Hildebrand, J. H. *J. Am. Chem. Soc.* **1949**, *71*, 2703.
(26) Crow, D. R. *Polarography of Metal Complexes*; Academic: London, 1969.

Table II. Stability Constants of *N*-MeIm Complexes in CH_2Cl_2 Containing 0.1 M $(TBA)ClO_4$

product	log K_1[a,c] (eq 1)	log K_2[b,c] (eq 2)	log K_1^-[a,d] (eq 4)	log K_2^-[a,d] (eq 5)	log K_1^{2-}[a,d] (eq 6)
$(TPP)InSO_3Ph$	5.7	3.3	8.1	2.3	10.7
$(TPP)InSO_3CH_3$	5.5	3.3	8.0	2.1	10.0
(TPP)InCl		1.0			
(TPP)InOAc		0.8			
$(OEP)InSO_3Ph$	5.2	3.0	6.2	2.2	
$(OEP)InSO_3CH_3$	5.3	3.0	6.7	2.1	
(OEP)InCl		1.2			
(OEP)InOAc		0.7			

[a] Good to ±0.4 log unit. [b] Good to ±0.2 log unit. [c] Values determined spectrophotometrically in ref 10. [d] Values determined from combined spectrophotometric and electrochemical data.

Scheme I

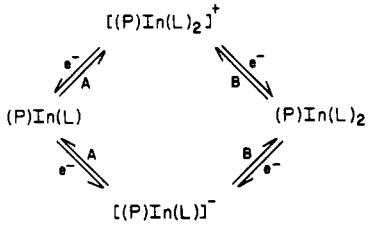

and $E_{1/2} = -0.99$ V. However, in this region the second reduction (peak IV) shifts by −65 mV with a tenfold increase in *N*-MeIm concentration. These shifts of $E_{1/2}$ are internally self-consistent between the two regions and can only be accounted for by the sequence of electron-transfer reactions shown in Scheme I, where A and B represent the region of *N*-MeIm concentration where a given electrode reaction predominates.

In region A, the neutral In(III) complex is bisligated while both the (P)In(L) anion radical and $[(P)In(L)]^-$ dianion are monoligated. The theoretical[26] shifts of $\Delta E_{1/2}/\Delta$ log (L) for reactions III and IV are −59 and 0 mV and the experimentally observed values are −66 and −10 mV, respectively. In region B, the neutral and anionic In(III) species are bisligated while the dianion exists as a mono(methylimidazole) complex. For this case, the theoretical $\Delta E_{1/2}/\Delta$ log (L) for reduction peaks III and IV are 0 and −59 mV and experimentally observed values of 0 and −65 mV are obtained. (See Figure 2.)

Formation Constants for *N*-MeIm Addition to $[(P)InX]^-$ and $[(P)InX]^{2-}$. Formation constants for ligand binding by metalloporphyrins have often been determined by monitoring electrochemical shifts of half-wave potential such as those shown in Figure 2. The exact method of calculation is generally described in ref 26 and is given in more detail in ref 27 for the case of iron porphyrins. Stability constants for both the neutral and the reduced complexes can often be determined from the electrochemical data alone, but in some cases, a combination of spectroscopic and electrochemical methodologies must be utilized.[6,27,28] Ligand binding by indium porphyrins involves this latter case.

Three different sets of half-wave potentials were utilized in the calculation of indium porphyrin stability constants. They were values of $E_{1/2}$ for (i) the reduction of $[(P)In(N\text{-MeIm})_2]^+$ to generate (P)In(*N*-MeIm) (region A, Figure 2), (ii) the reduction of $[(P)In(N\text{-MeIm})_2]^+$ to generate $(P)In(N\text{-MeIm})_2$ (region B, Figure 2), and (iii) the reduction of (P)In(*N*-MeIm) to generate $[(P)In(N\text{-MeIm})]^-$ (region A, Figure 2). In addition, values of K_1, K_2, and β_2, which were previously determined,[10] were used to calculate the formation constants for addition of *N*-MeIm to singly reduced $[(P)InX]^-$ and doubly reduced $[(P)InX]^{2-}$. These latter values were calculated from plots of the type shown in Figure 2 and are summarized in Table II.

It is interesting to note that the strength of the In(III)–*N*-methylimidazole complex increases with an increased negative charge on the porphyrin π ring system. For example, the value

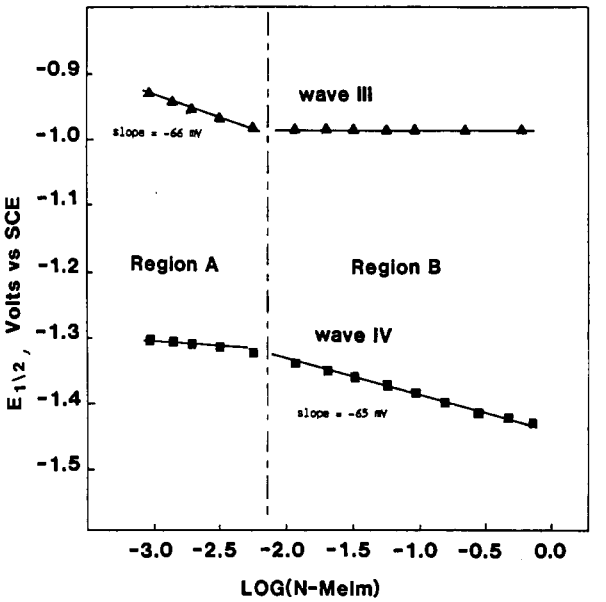

Figure 2. Dependence of $E_{1/2}$ on *N*-MeIm concentration for the first and second reductions of $(TPP)InSO_3Ph$ in CH_2Cl_2/*N*-MeIm mixtures. The two reductions correspond to peaks III and IV shown in Figure 1.

of log (K_1K_2) for addition of *N*-MeIm to $(TPP)InSO_3Ph$ is 9.0 while log (K_1K_2) for addition of the *N*-MeIm to $[(TPP)InSO_3Ph]^-$ and $[(TPP)InSO_3Ph]^{2-}$ is 10.4 and 10.7, respectively. The anion must be displaced from the In(III) prior to bisadduct formation. Thus, since a stronger In–X bond is present for the neutral complex than for the singly reduced complex, an increased value of log (K_1K_2) for the singly and doubly reduced species is reasonable. The increases in log K_1 from $(TPP)InSO_3Ph$, to $[(TPP)InSO_3Ph]^-$ and to $[(TPP)InSO_3Ph]^{2-}$ are 2.4 and 2.6 log units, respectively; this is a reflection of the progressively weaker In–SO_3Ph bond.

Electrochemistry of (P)InOAc and (P)InCl in the Presence of *N*-MeIm. (TPP)InCl is reduced in CH_2Cl_2, 0.1 M $(TBA)ClO_4$ by two one-electron-transfer processes that occur at −1.09 and −1.48 V.[14] A similar electrochemical behavior is observed for (TPP)InOAc, which is reduced at −1.12 and −1.49 V in CH_2Cl_2. The reduction potentials for both of these compounds are almost identical with the two reduction potentials observed for (TPP)-$InSO_3Ph$ and $(TPP)InSO_3CH_3$. This is shown in Table I, which lists $E_{1/2}$ for each of the investigated complexes in CH_2Cl_2 and in CH_2Cl_2/*N*-MeIm mixtures.

Both (TPP)InOAc and (TPP)InCl have an electrochemical behavior in CH_2Cl_2/*N*-MeIm mixtures different from that of $(TPP)InSO_3Ph$ and $(TPP)InSO_3CH_3$. The differences are due to the different strengths of the In–X bond[10] and are demonstrated by the voltammograms recorded during the titration of (TPP)InCl with *N*-methylimidazole. In the absence of *N*-methylimidazole, two well-defined reductions are observed. These are labeled as processes I and II in Figure 3a. Upon addition of 9 equiv of *N*-MeIm, the reoxidation peak of process II shifts positively by about 100 mV from that in the absence of ligand (see Figure 3a,b). In addition, a new reduction peak appears as a shoulder on the second reduction peak (see arrow, Figure 3b). These two reduction

(27) Kadish, K. M. In *Iron Porphyrins*; Lever, A. B. P., Gray, H. B., Eds.; Addison-Wesley: Reading, MA, 1983; pp 161–249.
(28) Kadish, K. M.; Shiue, L. R.; Rhodes, K. M.; Bottomley, L. A. *Inorg. Chem.* **1981**, *20*, 1274.

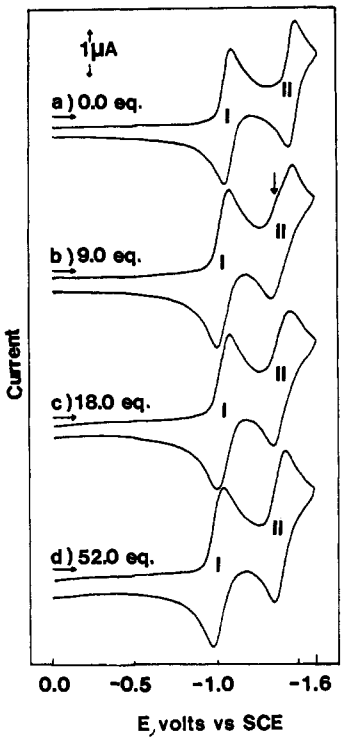

Figure 3. Cyclic voltammograms of 0.7×10^{-3} M (TPP)InCl in CH_2Cl_2, 0.1 M $(TBA)ClO_4$ containing the following equivalents of *N*-MeIm: (a) 0; (b) 9; (3) 18; (d) 52. The arrow in Figure 3b indicates the appearance of a new process at low *N*-MeIm concentrations.

peaks coalesce when log (*N*-MeIm) is higher than −1.30, and under these conditions a well-defined wave is again observed for process II.

The positively shifted reoxidation peak at low *N*-MeIm concentration (Figure 3b) suggests loss of Cl^- after addition of a second electron to $[(P)InCl(N\text{-MeIm})]^-$. However, in the presence of (TBA)Cl, the Cl^- remains bound to the reduction product. This was ascertained by monitoring cyclic voltammograms during the addition of Cl^- (in the form of (TBA)Cl) to a CH_2Cl_2/N-MeIm solution containing 1.5×10^{-2} M *N*-MeIm. Upon small addition of Cl^-, the oxidation peak coupled to the second reduction moves toward more negative potentials until a reversible wave is obtained in solutions containing greater than 80 equiv of Cl^-. Under these conditions, the second electrode reaction involves $[(P)InCl(N\text{-MeIm})]^-$ and $[(P)InCl]^{2-}$. The first electrode reaction involves (P)InCl(*N*-MeIm) and $[(P)InCl(N\text{-MeIm})]^-$ and no changes in $E_{1/2}$ of the first reduction are observed during Cl^- additions.

Reduction potentials of (TPP)InCl in CH_2Cl_2/N-MeIm mixtures can be correlated to the *N*-MeIm concentration as shown in Figure 4. This figure is divided into three regions. In region A, (TPP)InX(*N*-MeIm) is the primary indium complex in solution while in the second and third regions (regions B and C) $[(TPP)In(N\text{-MeIm})_2]^+$ is formed and is reduced at the electrode surface. After the addition of 2 equiv of *N*-MeIm, the first reduction of (TPP)InCl (peak I) shifts from −1.07 V (see Table I) to −1.04 V and remains constant up to log (*N*-MeIm) ≈ −1.5 (Figure 4, region A). This 30-mV shift is due to the formation of (TPP)InX(*N*-MeIm).[10] At higher *N*-MeIm concentrations (region B, Figure 4), peak I shifts positively by +67 mV per each tenfold increase in *N*-MeIm concentration. Finally, in region C [log (L) > −0.9] the half-wave potential for peak I remains constant at −0.99 V. This value is given in Table I, which lists the $E_{1/2}$ values of each complex in 1 M *N*-methylimidazole.

Similar voltammetric results were obtained for all four (P)InCl and (P)InOAc complexes in CH_2Cl_2/N-MeIm mixtures, thus suggesting similar reduction mechanisms. The shifts of $E_{1/2}$ in Figure 4 and the data presented in Figure 3, as well as the data for the other (P)InCl and (P)InOAc complexes, are self-consistent and are explained by the oxidation–reduction mechanism shown in Scheme II, where X = Cl^- or OAc^-, L = *N*-MeIm, and A, B, or C indicates the region of *N*-MeIm concentration where a specific electrode mechanism predominates.

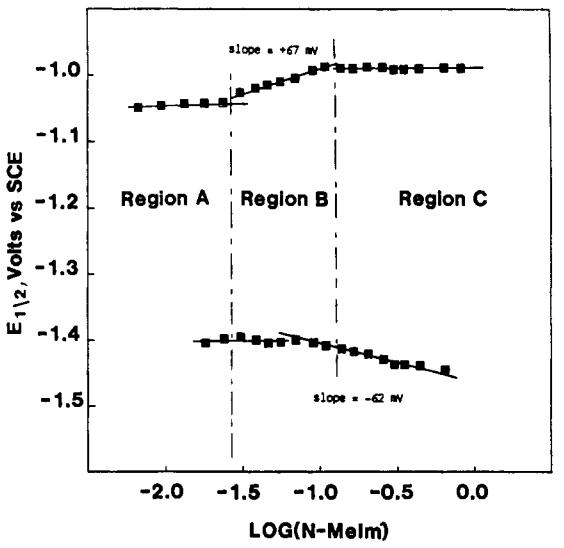

Figure 4. Dependence of $E_{1/2}$ on *N*-MeIm concentration for the first and second reductions of 0.9×10^{-3} M (TPP)InCl in CH_2Cl_2/N-MeIm mixtures.

Scheme II

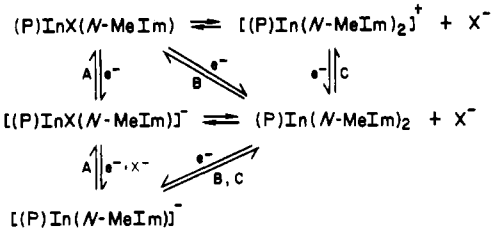

At low *N*-MeIm concentration, (P)InX(*N*-MeIm) is formed in solution and this species is reduced to either $[(P)InX(N\text{-MeIm})]^-$ (region A) or $(P)In(N\text{-MeIm})_2$ (region B). At higher *N*-MeIm concentrations (region C), the halide is displaced from $[(P)InX(N\text{-MeIm})]$ and $[(P)In(N\text{-MeIm})_2]^+$ is formed in solution. Under these conditions the reduction sequence proceeds via the singly reduced $[(P)In(N\text{-MeIm})_2]$, which then is reduced by a second electron to give $[(P)In(N\text{-MeIm})]^-$. Thus, the same monoligated $[(P)In(N\text{-MeIm})]^-$ dianion is formed in all three reaction sequences either via (P)InX(*N*-MeIm) (region A) or via $(P)In(N\text{-MeIm})_2$ (regions B and C).

Electrochemistry of $(P)InSO_3CH_3$ in CH_2Cl_2/py Mixtures. Stepwise formation of $(P)InSO_3R(py)$ and $[(P)In(py)_2]^+$ occurs upon addition of pyridine to CH_2Cl_2 solutions of $(P)InSO_3R$. Stability constants for formation of $(P)InSO_3R(py)$ have been estimated to be greater than 10^6 by ^1H NMR studies while stability constants for formation of $[(P)In(py)_2]^+$ from $(P)InSO_3R(py)$ range between log K_2 = 1.6 and 2.1.[10]

The addition of pyridine to $(TPP)InSO_3CH_3$ is qualitatively similar to that for addition of *N*-MeIm to $(TPP)InSO_3Ph$ (see Figure 1). They differ, however, in that the final value of $E_{1/2}$ for peak III (peak designation is the same as in Figure 1) is shifted positively with increased pyridine concentration (from −0.91 V in CH_2Cl_2 containing 1 equiv of pyridine to −0.87 V in 1 M pyridine) while, in CH_2Cl_2 containing *N*-MeIm, a negative shift in $E_{1/2}$ is observed (from −0.94 in CH_2Cl_2 containing 3 equiv of *N*-MeIm to −0.99 V in 1 M *N*-MeIm).

While peak III shifts positively by only 40 mV with increase of the pyridine concentration, $E_{1/2}$ for the second reduction (peak IV) shifts negatively by 65 mV for each tenfold increase of the pyridine concentration. These shifts may be accounted for by the mechanism shown in Scheme III where X = $SO_3CH_3^-$.

Both $(TPP)InSO_3CH_3(py)$ and $[(TPP)In(py)_2]^+$ are in solution when the concentration of pyridine is less than about 0.07 M. However, as the concentration of py is increased above 0.1 M,

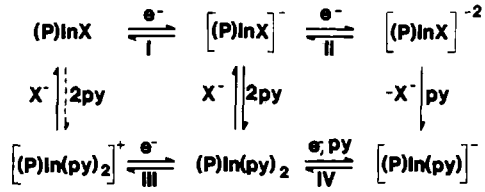

Figure 5. Pathways for reduction of (P)InX in pyridine.

Scheme III

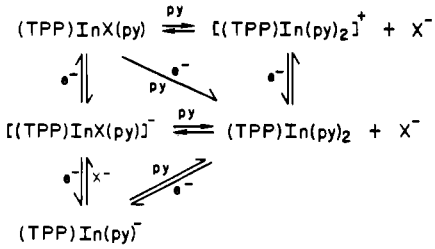

the equilibrium is shifted and $[(TPP)In(py)_2]^+$ becomes the only In(III) species in solution. This is demonstrated by the fact that two new reduction processes are observed (peaks III and IV) while the original two reductions (peaks I and II) have disappeared.

The 40-mV shift of the first reduction peak suggests that the first reduced product is a mixture of $[(TPP)InSO_3CH_3(py)]^-$ and $(TPP)In(py)_2$ during the electron-transfer step. However, the bisadduct is the ultimate product at longer time scales and this species is reduced during the second reduction. During this reduction, $(TPP)In(py)_2$ loses a pyridine molecule to give $[(TPP)In(py)]^-$. The loss of the second pyridine molecule is the cause of the −65-mV shift of wave IV.

Electrochemistry of (P)InX in Pyridine Where X = $SO_3CH_3^-$, Cl^-, and OAc^-. The electron-transfer mechanism of (P)InX in pyridine is given in Figure 5, and typical cyclic voltammograms of the (P)InX complexes in neat pyridine, 0.1 M $(TBA)ClO_4$, are shown in Figure 6. The four SO_3R derivatives (R = CH_3, Ph) exhibit two reversible electron transfers in neat pyridine, and these reactions correspond to the reductions of $[(P)In(py)_2]^+$ and $(P)In(py)_2$.

The first reduction of (P)InX is irreversible when X = Cl^- or OAc^-, and depending upon the complex, there may be either one or two reoxidation peaks on the reverse scan (see Figure 6). The second reduction is reversible for voltammograms measured at room temperature and at scan rates lower than 1 V/s. In addition, the values of $E_{1/2}$ for the second reduction of each compound in the OEP or TPP series are invariant, independent of the counterion on (P)InX. For example, the second reduction of (TPP)InX occurs at −1.30 V for all four of the TPP complexes while the second reduction of (OEP)InX occurs at −1.64 V for all four of the OEP complexes. This suggests that a rapid loss of Cl^- from $[(P)InCl]^-$ occurs after the addition of one electron and that the second electron transfer involves the $(P)In(py)_2/[(P)In(py)]^-$ couple.

The scan rate dependence of E_{pc} and E_{pa} for reduction of the four chloro and acetate complexes is consistent with the "box" mechanism in Figure 5. For the four compounds the cathodic and anodic peaks shift by 30 mV per tenfold increase in scan rate. This suggests an EC mechanism[29] (electron transfer followed by a chemical reaction) for both the reduction and the reoxidation processes.

In order to further confirm the overall mechanism shown in Figure 5, variable-temperature electrochemistry was performed with both the (P)InOAc and (P)InCl derivatives. A similar temperature dependence was observed for the four (P)InX complexes (where X = Cl^- and OAc^-) in pyridine containing 0.1 M $(TBA)ClO_4$. These results are shown in Figure 7 for (TPP)InCl reduction at a scan rate of 0.5 V/s. Three reduction and two reoxidation peaks are observed at 21 °C, but at −10 °C there are four reduction and two reoxidation peaks. This suggests that all

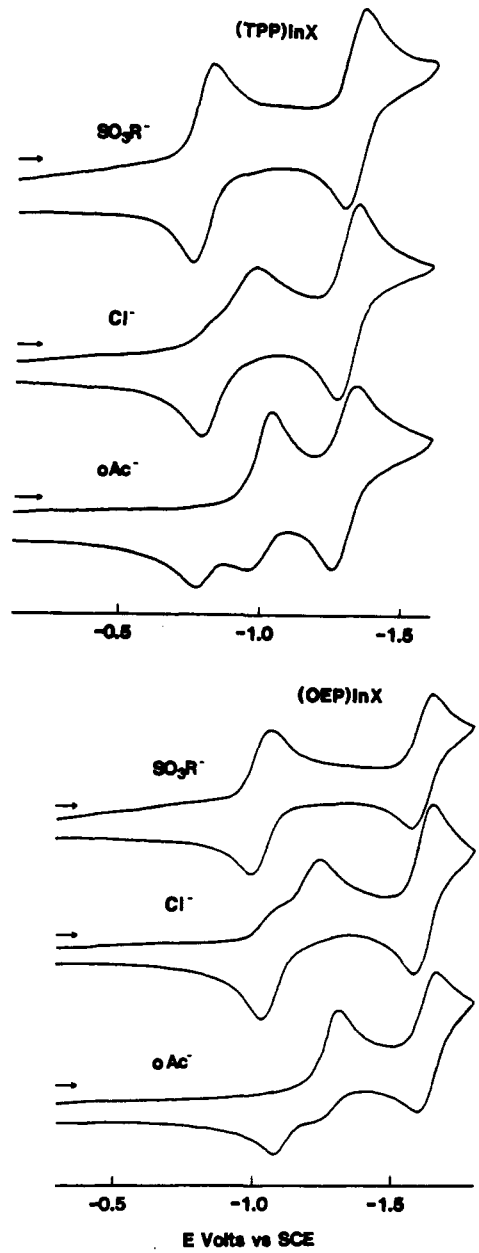

Figure 6. Cyclic voltammograms of the (P)InX complexes in neat pyridine containing 0.1 M $(TBA)ClO_4$.

six indium species in Figure 5 are present at −10 °C but that a rapid dissociation of X^- occurs after formation of both $[(P)InX]^-$ and $[(P)InX]^{2-}$. This also suggests that the reoxidation proceeds from $[(P)In(py)]^-$ to $[(P)In(py)_2]^+$ via the lower pathway in Figure 5. However, at −40 °C, the electrogenerated $[(P)InX]^{2-}$ can be stabilized such that a reoxidation pathway via $[(P)InX]^-$ and (P)InX will occur during the time scale of the electrochemical experiment. This is illustrated by the cyclic voltammogram in Figure 7 (−40 °C).

The voltammogram at −40 °C confirms that all four electrode reactions in Figure 5 occur during the time scale of the experiment and that both the upper and lower pathways are followed. Under these conditions the values of $E_{1/2}$ for the upper pathway are −1.02 and −1.40 V, which are similar to the $E_{1/2}$ values of −1.09 and −1.48 V in CH_2Cl_2 at room temperature (see Table I). At −40 °C the two reductions of $[(TPP)In(py)_2]^+$ (lower pathway, Figure 5) occur at −0.80 and −1.28 V, and these values are similar to the $E_{1/2}$ values of −0.77 and −1.30 V for the room-temperature reduction of $(P)InSO_3R$ in neat pyridine (see Table I).

The mechanism shown in Figure 5 was also investigated as a function of increasing scan rate in the presence of excess X^-. This is shown in Figure 8, which gives cyclic voltammograms for the

(29) Nicholson, R. S.; Shain, I. *Anal. Chem.* **1964**, *36*, 706.

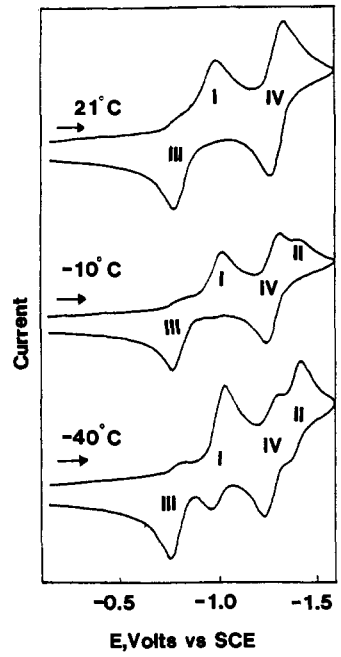

Figure 7. Variable-temperature cyclic voltammograms of (TPP)InCl in neat pyridine, 0.1 M $(TBA)ClO_4$ at a scan rate of 0.5 V/s.

Scheme IV

$$(OEP)InCl \overset{e^-}{\rightleftharpoons} [(OEP)InCl]^-$$

$$-2py \downarrow Cl^- \qquad 2py \downarrow Cl^-$$

$$[(OEP)In(py)_2]^+ \overset{e^-}{\rightleftharpoons} (OEP)In(py)_2$$

reduction of (OEP)InCl in pyridine containing 0.1 M (TBA)Cl. At 0.1 V/s, the first one-electron transfer of (OEP)InCl is quasi-reversible as evidenced by $\Delta E_p = \sim 75$ mV. However, as the scan rate is increased, the return oxidation peak splits into two peaks. Finally, at 10 V/s the more positive back-oxidation peak disappears and the reduction again becomes reversible. $E_{1/2}$ for the peak at 10 V/s is more negative (-1.21 V) than $E_{1/2}$ for the peak at 0.05 V/s (-1.15 V). This suggests the mechanism shown in Scheme IV.

The first reduction and reoxidation process involves the $(OEP)InCl/[(OEP)InCl]^-$ couple at both very slow and very fast scan rates. This is true despite the fact that $(OEP)In(py)_2$ is the predominant reduced species present in solution. $[(OEP)InCl]^-$ is more easily oxidized than $(OEP)In(py)_2$, and thus at slow scan rates, there is a shift of equilibrium prior to electron transfer (an electrochemical CE mechanism) such that the more easily oxidized species reacts. However, at scan rates between 0.5 and 4 V/s the reassociation of Cl^- cannot totally occur prior to reoxidation, and hence, two oxidation peaks are observed. Finally, only one set of coupled oxidation–reduction peaks is observed at 10 V/s, and at this scan rate there is no evidence for a peak corresponding to the oxidation of $(OEP)In(py)_2$. This suggests that the loss of Cl^- from $[(OEP)InCl]^-$ does not occur on the electrochemical time scale. This is consistent with the results at -40 °C (in the absence of excess Cl^-, Figure 7) and suggests that the reversible electrode reaction is given by eq 7 at all scan rates.

$$(OEP)InCl + e^- \rightleftarrows [(OEP)InCl]^- \qquad (7)$$

Similar electrochemical behavior was observed for (OEP)InOAc in CH_2Cl_2 containing 0.1 M (TBA)OAc as well as for the (TPP)InX derivatives in CH_2Cl_2 containing 0.1 M (TBA)X. However, the type of scan rate dependence shown in Figure 8 could only be seen for the TPP derivatives at reduced temperature. For example, similar types of current–voltage curves were not observed for (TPP)InCl until the temperature was reduced to near 0 °C. This implies the rate for dissociation and reassociation of Cl^- is larger for $[(TPP)InCl]^-$ than for $[(OEP)InCl]^-$. Such differences

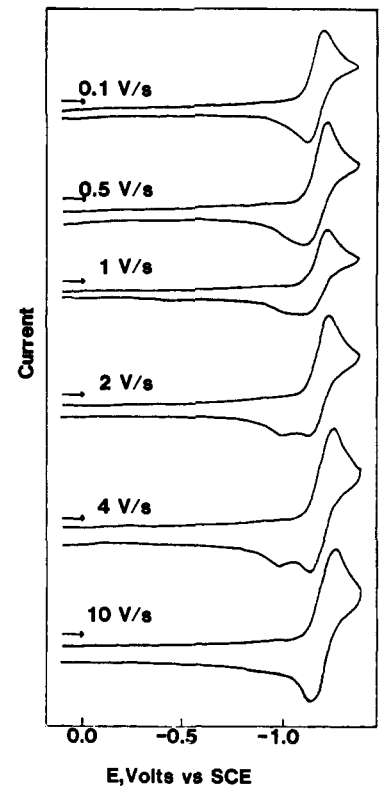

Figure 8. Room-temperature cyclic voltammograms of (OEP)InCl as a function of scan rate in pyridine, 0.1 M (TBA)Cl.

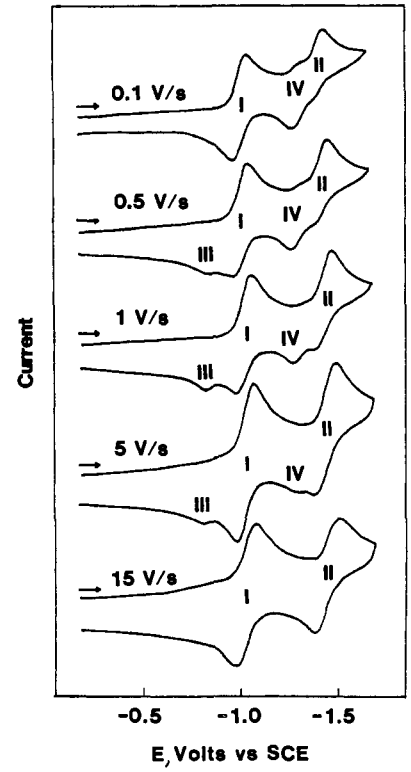

Figure 9. Cyclic voltammograms of 1×10^{-3} M (TPP)InCl in pyridine, 0.1 M (TBA)Cl, at -35 °C.

between the TPP and the OEP derivatives are not unexpected and can be explained by comparing the steric hindrance of the TPP system with the relatively sterically free OEP system.

Cyclic voltammograms of (TPP)InCl in pyridine containing 0.1 M (TBA)Cl at -35 °C are shown in Figure 9 as a function of scan rate. These voltammograms are qualitatively and quantitatively similar to the voltammograms in Figure 7 and further

support the electron-transfer scheme shown in Figure 5. In the presence of 0.1 M Cl^-, the first reduction involves (P)InCl and $[(P)InCl]^-$ while the second reduction involves both $[(P)InCl]^-$ and $(P)In(py)_2$, which is formed after Cl^- dissociation. This is illustrated by the voltammogram at 0.1 V/s. At 15 V/s, dissociation of Cl^- does not occur during the time scale of the measurement and only the top set of electrode reactions in Figure 5 take place. At all other scan rates, intermediate behavior is observed, and between two and four oxidation peaks are obtained depending upon scan rate.

In conclusion, the electrochemical studies are consistent with the ligand-addition reactions reported earlier for the (P)InX system.[10] The formation of a mono- and bis(*N*-methylimidazole) adduct is observed by electrochemistry for all of the neutral compounds but the formation of bis(pyridine) adducts is observed only for the SO_3R^- derivatives. The electrochemistry also provides information on nitrogenous base addition to the species formed after reduction by one or two electrons. In the presence of pyridine or *N*-MeIm the formation of $[(P)InX(L)]^-$ or $(P)In(L)_2$ is observed after reduction by one electron. The exact species formed is dependent upon both the nature of the axial ligand and the ligand concentration. However, after the addition of a second electron to $[(P)InX(L)]^-$ or $(P)In(L)_2$, a pentacoordinated indium porphyrin dianion is always formed.

Acknowledgment. The support of the National Science Foundation (Grant CHE-8215507) is gratefully acknowledged.

Registry No. *N*-MeIm, 616-47-7; (TPP)$InSO_3Ph$, 70619-92-0; (TPP)$InSO_3CH_3$, 70619-88-4; (TPP)InCl, 63128-70-1; (TPP)InOAc, 96150-61-7; (OEP)$InSO_3Ph$, 70619-98-6; (OEP)$InSO_3CH_3$, 70619-94-2; (OEP)InCl, 32125-07-8; (OEP)InOAC, 96150-60-6; (TPP)$InSO_3Ph$(*N*-MeIm), 102614-85-7; (TPP)$InSO_3Me$(*N*-MeIm), 102648-59-9; (OEP)$InSO_3Ph$(*N*-MeIm), 102614-86-8; (OEP)$InSO_3Me$(*N*-MeIm), 102630-10-4; $[(TPP)In(N\text{-MeIm})_2]^+$, 102614-87-9; $[(OEP)In(N\text{-MeIm})_2]^+$, 102614-88-0; pyridine, 110-86-1.

Contribution from the Department of Chemistry, University of Missouri—St. Louis, St. Louis, Missouri 63121

Circularly Polarized Luminescence from Racemic Lanthanide(III) Complexes with Achiral Ligands in Aqueous Solution Using Circularly Polarized Excitation

Gary L. Hilmes and James P. Riehl*

Received December 18, 1985

The circularly polarized luminescence (CPL) and total luminescence (TL) spectra are reported for aqueous solutions of tris complexes of Tb(III), Eu(III), Sm(III), and Dy(III) with 2,6-pyridinedicarboxylic acid in basic media. The optical activity is generated from these *racemic* solutions by using as the excitation source circularly polarized Ar ion laser lines. No CPL was observed from similarly prepared solutions of Tb(III), Eu(III), and Sm(III) with oxydiacetic acid. CPL was measured for the aqueous complex of Dy(III) with oxydiacetic acid. These results are interpreted in terms of the kinetic stability of the complexes formed, and comparisons are made with other optical and with NMR measurements.

Introduction

Spectroscopic interest in the study of complexes of lanthanide ions has increased significantly in the last 10 years primarily because of the use of a number of these species as NMR shift reagents[1] and as optical probes of biomolecular structure.[2,3] Several lanthanide ions have been shown, for example, to replace spectroscopically inert Ca(II) (and sometimes Mg(II)) in a number of important biomolecular systems, such as calcium-binding proteins, while retaining, at least partially, their associated biological activity.[2-4] The intraconfigurational 4f–4f electronic transitions of lanthanide ions are generally very sensitive to the coordination environment around the lanthanide ion. The optical spectroscopy of these f–f transitions may involve several different free-ion states that are well-separated in energy. In addition, each electronic band may be composed of a number of possible individual crystal field transitions. For these reasons, the lanthanide ions are considered to be potentially important tools for the study of biomolecular systems, particularly if theoretical formalisms or models relating the observed spectra to specific aspects of molecular structure can be developed. The present work is a contribution toward such an understanding. Almost all of the emission studies on lanthanides in solution have involved either Tb(III) or Eu(III), both of which emit strongly even in solution at room temperature, to a number of different well-resolved electronic states.[2] Generally, excitation of the lanthanide is achieved via absorption in the ultraviolet region by either the ligand or metal ion, but the 4f–4f absorption bands can also be excited directly by using visible region laser excitation.

The measurement of the circularly polarized luminescence (CPL) in the emission spectra of lanthanide ions has been shown to be a very important probe of the structure of lanthanide complexes.[5,6] The development of useful and reliable spectra–structure relationships in CPL from lanthanide(III) ions has to some extent been hindered by the lack of spectral measurements for systems in which the structure is known. In particular, much of the CPL work that has been reported on lanthanide complexes with *chiral* ligands yields only indirect and, in most cases, only speculative conclusions concerning the structure of these complexes in aqueous solution. One is never really able to separate completely effects due to the configuration of ligands about the central ion from effects due to chelate ring conformations or so-called vicinal effects. These latter effects arise from the existence of asymmetric centers on inherently chiral ligands. Very little CPL data exist for complexes that are chiral due solely to the configuration of *achiral* chelate rings about the lanthanide ion. There have been measurements of CPL from a limited number of *crystals* in which the lanthanide complexes crystallize in enantiomorphic space groups.[7,8] There has also been a fairly large amount of work reported on CPL from aqueous solutions of Tb(III) with 2,6-pyridinedicarboxylic acid (dipicolinic acid, DPA) in which a chiral species has been added or a chiral solvent used.[9] This complex has been shown to possess D_3 geometry in the solid state.[10-12] Much of the solution CPL work has been concerned with the nature of the coordination or perturbation caused by the additional chiral component. A considerable amount of this work has been described as examples of the so-called "Pfeiffer effect",[13,15] al-

(1) *Nuclear Magnetic Shift Reagents*; Sievers, R. E., Ed.; Academic: New York, 1973.
(2) Richardson, F. S. *Chem. Rev.* **1982**, *82*, 541.
(3) Horrocks, W. D., Jr.; Sudnick, D. R. *Acc. Chem. Res.* **1981**, *14*, 384.
(4) Brittain, H. G.; Richardson, F. S.; Martin, R. B. *J. Am. Chem. Soc.* **1976**, *98*, 8255.
(5) Richardson, F. S.; Riehl, J. P. *Chem. Rev.* **1977**, *77*, 773.
(6) Riehl, J. P.; Richardson, F. S. *Chem. Rev.*, in press.
(7) Morley, J. P.; Saxe, J. D.; Richardson, F. S. *Mol. Phys.* **1982**, *47*, 379.
(8) Saxe, J. D.; Morley, J. P.; Richardson, F. S. *Mol. Phys.* **1982**, *47*, 407.
(9) Brittain, H. G. *Coord. Chem. Rev.* **1983**, *48*, 243.
(10) Albertsson, J. *Acta Chem. Scand.* **1970**, *24*, 213.
(11) Albertsson, J. *Acta Chem. Scand.* **1972**, *26*, 985.
(12) Albertsson, J. *Acta Chem. Scand.* **1972**, *26*, 1023.

0020-1669/86/1325-2617$01.50/0